JOURNAL OF THERMOPHYSICS AND HEAT TRANSFER
Vol. 24, No. 4, October–December 2010

Heat Transfer Distribution of Semicylindrical Concave Surface Impinged by Circular Jet Rows

S. Nagesh Yasaswy,* Vadiraj. V. Katti,† and S. V. Prabhu‡
Indian Institute of Technology, Bombay, Mumbai 400076, India

DOI: 10.2514/1.48218

The impingement cooling of the leading edge of a gas turbine airfoil is modeled by considering impingement of three rows of jets on a semicylindrical concave surface. Experimental investigations are conducted to study the influence of jet-to-jet distance ($s/d = 2.83$, 4, and 6) and jet-to-plate distance ($z/d = 2$, 4, 6, and 8) on the local heat transfer of a semicylindrical concave surface impinged by three rows of multiple jets for different Reynolds numbers (12,000, 15,000, and 18,000). The local heat transfer coefficient is estimated using thermal images obtained by infrared thermal imaging technique. The local distribution of Nusselt numbers and the overall average Nusselt numbers were computed and compared. It was observed that the local heat transfer coefficients at $\theta = 0°$ decrease with increase in z/d, whereas the heat transfer coefficients at $\theta = 60$ and 80° increase with an increase in z/d at all Reynolds numbers. The configuration with $s/d = 2.83$ and $z/d = 4$ is observed to have the maximum heat transfer distribution with minimum coefficient of variance compared to other configurations at all Reynolds numbers covered in this study.

Nomenclature

D	=	diameter of target plate, m
D_1	=	jet-tube diameter, m
d	=	diameter of jet hole, m
h	=	heat transfer coefficient, W/m^2K
$\dot{m}_j$	=	mass flow rate through each jet, kg/s
$\dot{m}$	=	total mass flow rate, kg/s
Nu	=	Nusselt number
Q	=	volumetric flow rate, m^3/s
q''	=	heat flux, W/m^2
Re	=	Reynolds number
s	=	jet-to-jet spacing, m
T_j	=	jet-air temperature, °C
T_w	=	wall temperature, °C
y	=	longitudinal distance from stagnation point, m
z	=	jet-to-plate spacing, m
μ	=	dynamics viscosity of air, Pa · s

I. Introduction

MULTIPLE-JET impingement is desirable when large surface areas require cooling or heating. Major applications of these are found in gas turbine blade cooling. Cool air from the multiple jets impinge on the internal surfaces of the blades so that the gas turbine cycle may be operated with higher inlet gas temperatures for higher efficiencies. The leading edge of the gas turbine is severely influenced by the impacting hot gases. Hence, the leading edge needs to be effectively cooled. The internal passage at the leading edge may be considered to have a semicircular concave surface and this region may be convectively cooled by a spanwise row of impinging jets.

The impinging jets are one of the better methods of cooling the leading edge of the gas turbine blades, due to their inherent characteristics of high rates of heat transfer from short flow paths. The airfoils are cast hollow. A jet tube, which has a series of holes machined into it, is placed in the hollow airfoil with its orientation such that the holes are opposite to the inside surface of the leading edge. The cooling air is introduced into the jet tube at the base of the airfoil. Air exits through a series of jet holes directed to the leading edge of the airfoil and impinges on the inside surface of the airfoil. The spent air leaves the airfoil at its trailing edge after picking up heat from the airfoil. The cooling performance is influenced by the jet Reynolds number, the jet-to-jet distance (s/d), the relative curvature of the concave surface (D/d), and the distance of the leading edge from the nozzle exit (z/d).

Several investigators reported studies on heat transfer and fluid flow distribution with impinging jets on curved surface simulating leading edge of the gas turbine blade. Impingement by a single row of circular jets goes way back to Chupp et al. [1], who reported the stripwise-averaged heat transfer distribution due to impingement of a row of circular jets on the cylindrical concave surface. They provided correlations for heat transfer coefficients at the stagnation strip and average heat transfer coefficients in terms of Reynolds number and nondimensional geometric parameters of the configuration such as surface curvature, pitch, and jet-to-plate distance. Metzger et al. [2] conducted experiments to study heat transfer characteristics due to impingement of a row of circular jets on a cylindrical concave surface for a curvature ratio $D/d = 8.34$ and $s/d = 1.67$, 3.33, and 6.67. Heat transfer coefficient was measured using a transient response of a thermal sensor made of aluminum with a thermocouple embedded in it. They reported that maximum heat transfer rates are possible with $z/d = 1$ for any of the configurations investigated. They gave a correlation for maximum average Stanton number for Reynolds number varying from 1150–6300. Metzger et al. [3] experimentally studied the heat transfer characteristics of impingement into cavities that model the cooled leading edges of gas turbine engine airfoils. The influence of elongated leading edge was to decrease the overall heat transfer. Correlations were provided for maximum heat transfer rates for an optimum position of jet nozzle on the curved surface. Jusionis [4] studied the influence of gas flow rate, the jet-to-plate distance and the angle of inclination of the jet on the heat transfer distribution of multiple jet impingement on enclosed concave surface. He suggested a correlation for average Nusselt number based on Reynolds number, jet-to-jet spacing, jet-to-plate distance and curvature of concave surface. Tabakoff and Clevenger [5] compared three different systems of air jets impinging on a semicylindrical surface. A slot jet, a row of round jets, and a square array of round jets were used for comparison. The best heat transfer performance was observed for the case of round-jet array followed by the row of round jets. Bunker and Metzger [6] used scaled-down models of turbine blade leading-edge regions for impingement cooling. Cooling is provided by a single line of equally spaced

Received 21 November 2009; revision received 8 May 2010; accepted for publication 12 May 2010.

*Graduate Student, Mechanical Engineering Department.
†Research Scholar, Mechanical Engineering Department.
‡Associate Professor, Mechanical Engineering Department.

multiple jets aimed at the leading-edge apex and exiting the leading-edge region in the chordwise direction. Results indicated that the general increase in heat transfer with approximately the 0.6 power of jet Reynolds number, increase in heat transfer with decreasing leading-edge sharpness as well as with decreasing nozzle to apex distance and increase in spanwise average heat transfer with decreasing jet pitch to diameter ratio. They also reported that the heat transfer performance degrades severely in the leading edge for an equivalent slot jet. Iacovides et al. [7] studied the influence of rotation on the impingement cooling of curved surfaces. Water was used as the working fluid and liquid crystal thermography was used to study the heat transfer distribution. The experiments were carried out at a Reynolds number of 15,000 for clockwise, anticlockwise, and no rotation of the test section. For the nonrotating case the impingement of jets gave rise to rough concentric elliptical rings of uniform Nusselt numbers. Fenot et al. [8] studied the effect of multiple hot round jets on semicylindrical concave surface for Reynolds numbers varying from 10,000–23,000 and z/d ranging from 2–5. Nusselt number correlations were obtained as a function of jet-to-plate distances and curvature ratio. Hrycak [9] gave an expression to estimate stagnation and average heat transfer coefficients from a row of impinging jets on a concave cylindrical surface. The experiments were carried out for a curvature ratio of 13.3, $s/d = 6.67$ and Reynolds number varying from 2500–30,000. Taslim et al. [10,11] studied the curved surface impingement similar to the present case. Two mechanisms of inflows to the test section were studied and the outflow was either one-sided or nominal (two-sided). Two z/d of 5.2 and 6.2 with an s/d of 4 were studied. It was observed that the exit mechanism did not play a significant role in the heat transfer distribution on the curved surface. Both experimental and numerical investigations were carried out and compared. However, it was observed that the Nusselt numbers increase slightly when the inflow is one-sided for nominal or one-side exit cases. Rama Kumar and Prasad [12] studied the flow characteristics from multiple circular jets impinging on a concave surface. Both experimental and computational investigations were carried out and compared. The experiments were performed with a 30:1 scaled-up model, of the leading-edge zone of a gas turbine nozzle guide vane. The experiments were carried out for Reynolds number varying from 2850–28,476, z/d of 1, 4, and 6, and s/d of 2.7 and 5.4. k-ω shear stress transport model for turbulence closure was used for computational fluid dynamics (FLUENT) analysis. Literature review suggests that little information is available on the local heat transfer distribution due to the impingement of multiple rows of circular air jets on a cylindrical surface. Hence, the present work considers a configuration that not only simulates the impingement cooling system for cooling of the gas-turbine leading edge, but also reduces the nonuniformity of the local heat transfer coefficient on the leading edge of the gas turbine. Instead of a single row of jets that are machined centrally on the jet tube, three rows of impinging jets are machined where two of these rows are present at a 40° angle on either side of the centrally machined row of jets. Hence, an attempt is made to cool the leading edge of a gas turbine blade uniformly by employing three rows of multiple impinging jets. The influence of geometric parameters such as pitch s/d and jet-to-plate distance z/d on the local distribution of heat transfer are studied for different Reynolds numbers. The curvature ratio is kept constant at $D/d = 10$. Pitches s/d of 2.83, 4, and 6 and jet-to-plate distances z/d of 2, 4, 6, and 8 are studied. Jet Reynolds numbers of 12,000, 15,000, and 18,000 are considered for each of the configurations studied.

A schematic layout of the test facility is shown in the Fig. 1. The metered quantity of air is supplied to the jet tube of the test section from an air compressor through the calibrated Venturi meter. The air filter and the pressure regulator are installed upstream of the Venturi meter to filter out the air and to maintain the desired pressure at the Venturi meter. The flow rate to the test section is regulated by the valve located downstream of the Venturi meter.

II. Experimental Setup and Procedure

Figure 2 shows a detailed view of the test section. The jet tube has two parts. First part is the flow developing section called jet-tube inlet that has a rectangular cross section. This section is followed by a section called jet-tube main having rectangular cross section with rounded ends. One end of the jet-tube inlet is connected to the air line from the exit of the Venturi meter. The length of the jet-tube inlet is about 25 times its hydraulic diameter and long enough to achieve fully developed flow at the inlet of the jet-tube main. The other end of the tube is connected to the jet-tube main. The jet-tube main has three spanwise rows of uniform circular holes of diameter 3 mm drilled normal to the tube axis. In addition to the centrally machined row of jets, two more rows at an angle of 40° on either side of the central row of jets were machined on the jet tube. The semicircular concave target plate of 30 mm diameter is made of a thin foil of stainless steel (0.05 mm thick) and clamped at the ends in the bus bar. Because of the thinness of the foil, lateral conduction is negligible and surface provides constant heat flux situation. The interchangeable spacers are positioned between the ends of the jet-tube main and target plate to provide necessary jet-to-plate distance. These spacers also seal the passage for spent air flow of jets in the spanwise direction. The effective spanwise length of the semicylindrical concave target surface is fixed at 140 mm. The jet fluid is constrained to exit in the streamwise direction along the U-channel formed between the supporting acrylic frame, concave target surface, and supply main jet tube.

The thermal images are obtained from an infrared camera positioned on the backside of the concave target surface. The infrared camera shows the flat projected image of the concave target surface. Hence, while analyzing the thermal images the projected lengths of the curved surface and not the arc lengths were considered for the location of the jet impingement on the target surface for the case of jets present on either side of the centrally machined row of jets. One dimensional energy balance across the heated plate shows negligible temperature difference across it. Hence, the local temperature measured on the back surface is considered to be the same as that on the impingement plane or the front surface. The back side of the target surface i painted black using a thin coat of matte finish Asian paint, which provides a high-emissivity (0.99) surface. Infrared radiometry technique is used to measure local temperature from uniform heat flux surface, which provides higher special resolution of temperature

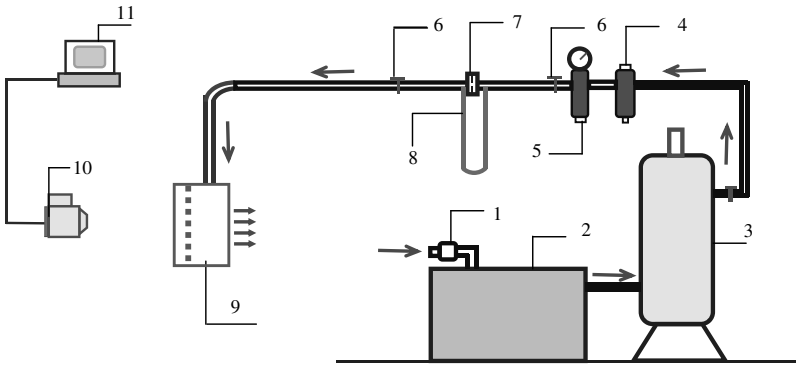

Fig. 1 Layout of the experimental setup.

Table 1 Configurations investigated in the present study

Pitch s/d	Number of jet holes	Jet-to-surface normal distance z/d	Reynolds number Re
2.83	45 (15 × 3)	2, 4, 6, 8	12,000, 15,000, 18,000
4.0	33 (11 × 3)	2, 4, 6, 8	12,000, 15,000, 18,000
6.0	21 (7 × 3)	2, 4, 6, 8	12,000, 15,000, 18,000

than thermocouples. A Thermoteknix Ti200 infrared thermal camera is used to collect local temperature distribution with a resolution of about 0.5 mm per pixel. Power is supplied from a dc power source. The voltage across the target plate is measured by Meco digital meter whose ranges and accuracies are of 0 to 20 ± 0.5% V. Suitable voltage taps are provided in each of the bus bars. The jet-air temperature is measured using a Chromel-Alumel thermocouple (K-type) positioned at the inlet of the nozzle. The tail end of the thermocouple is maintained in an ice bath made by crushed ice and water in a thermoflask with proper insulation. This produces a reference temperature of 0°C. The output of the thermocouple is measured by a Meco millivoltmeter. Power loss from the exposed surface of the target plate due to natural convection and radiation is estimated experimentally. The various configurations formed from the three jet tubes considered during the present study are given in Table 1.

III. Data Reduction

The jet Reynolds number is defined on the basis of jet-hole diameter and is estimated using Eq. (1):

$$Re = \frac{4\dot{m}_j}{\pi d \mu} \tag{1}$$

$$\dot{m}_j = \frac{\dot{m}}{\text{number of jets}} \tag{2}$$

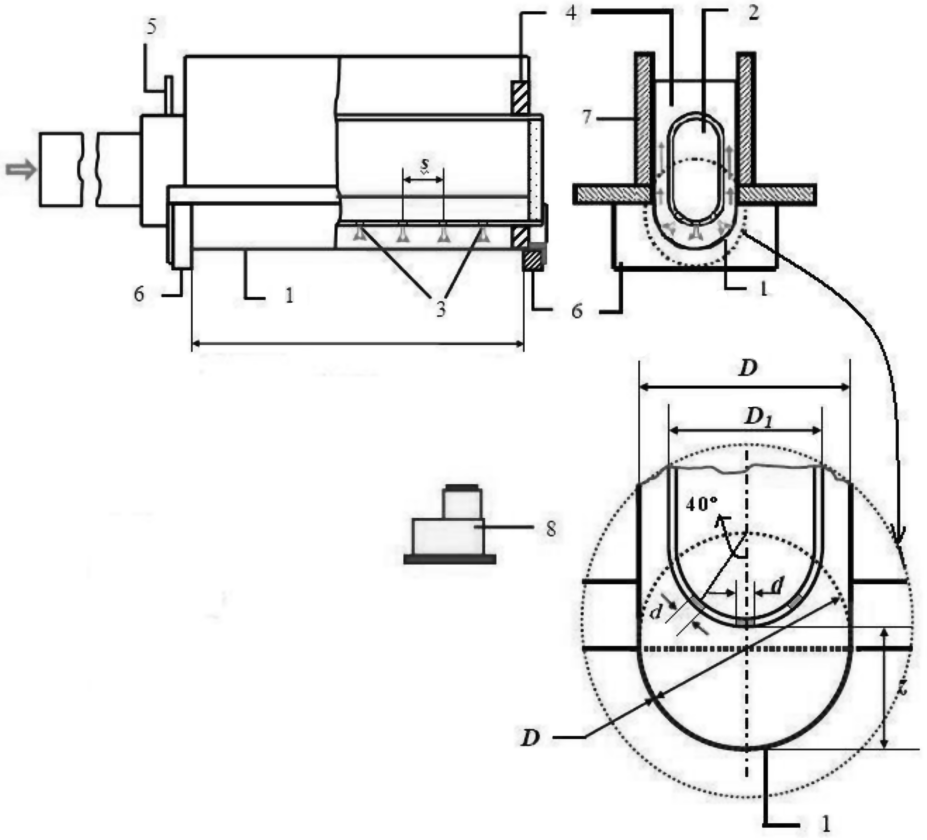

Fig. 2 Detailed view of the test section.

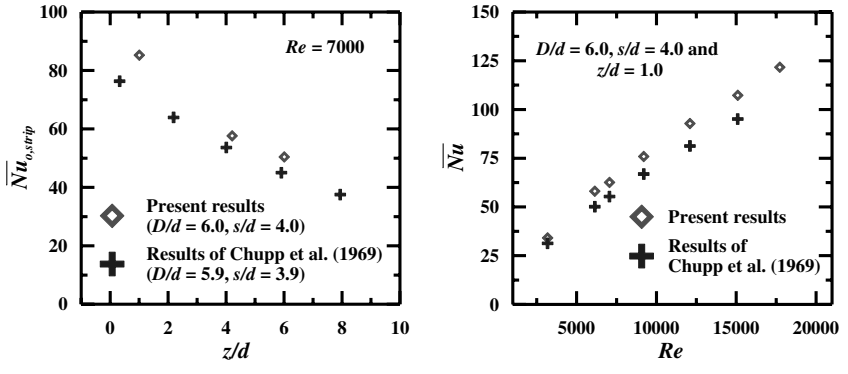

Fig. 3 Comparison of present results with the results of Chupp et al. [1].

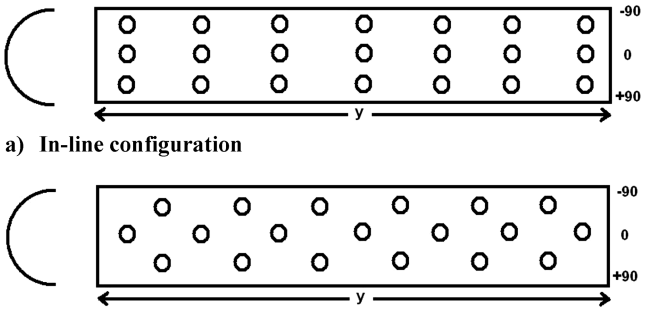

Fig. 4 Two different configurations of the jet tubes that were used in the present study.

For each configuration, the target surface temperature measurements are made under steady state conditions using the thermal images obtained from the infrared camera. The thermal images are digitized using VisIR Ti200 software. The plenum air temperature is used as the reference jet fluid temperature in all heat transfer calculations. The Nusselt number variation was observed to be within 15% if the adiabatic wall temperature was used as the reference jet fluid temperature rather than the plenum air temperature being used as the reference jet fluid temperature. A comparison of using both of these temperatures for the calculation of Nusselt numbers is shown in the Results and Discussions section. The local heat transfer coefficients are estimated based on Eq. (3):

$$h = \frac{q''}{T_w - T_j} \tag{3}$$

The uniformity of distribution of local Nusselt numbers may be quantified by defining a parameter called coefficient of variance (COV) and is expressed in percentage. The coefficient of variance of Nusselt numbers is defined as the ratio of standard deviation of the local Nusselt numbers to the corresponding average Nusselt number. Mathematically, it is given by Eq. (4):

$$\mathrm{COV}_{Nu} = 100 \times \frac{\sigma Nu}{\overline{Nu}} \tag{4}$$

The value of this parameter indicates the spread of the Nusselt number distribution about the average Nusselt number for a given configuration. The configuration, which produces higher heat transfer coefficients at lower values of COV_{Nu} may be identified as better one. Uncertainties in the measurement of Nusselt numbers are carried out using the method suggested by Moffat [13] and are around 4.4% for all the Reynolds numbers investigated.

IV. Validation

The present experimental setup is exactly similar to the one performed earlier using a single row of jets centrally machined on the jet tube impinging on a curved surface. This earlier configuration was similar to the one used by Chupp et al. [1], which simulates cooling of leading edge of a typical gas turbine blade. This configuration has a single row of seven jets ($s/d = 4.0$ and $D/d = 6.0$). The jet-to-surface distances of d, $4.2d$, and $6d$ are considered.

The local distribution of Nusselt numbers based on the jet-hole diameter are averaged stripwise. Each strip is of spanwise length of $7s$ and of arc length equal to one seventh of a semicircle in streamwise direction. Seven such segments are formed in the streamwise direction with three strips located each on either side of central stagnation strip. This is done because similar strip-averaged Nusselt numbers are reported by Chupp et al. [1]. Figure 3a shows the distribution of the stagnation-strip strip-average Nusselt number at different z/d for Reynolds number of 7000. These results and the

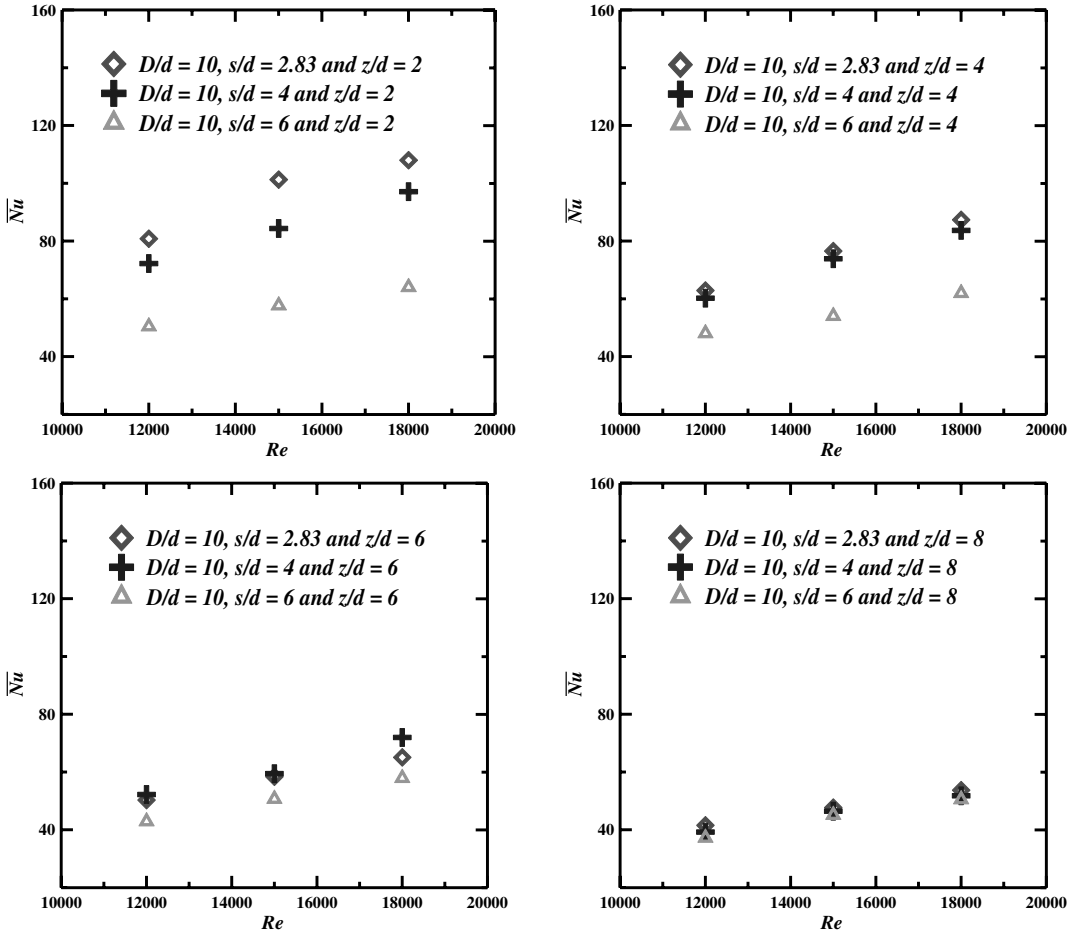

Fig. 5 Influence of pitch and Reynolds number on the average Nusselt numbers at different jet-to-plate distances.

Table 2 Average Nusselt numbers and their coefficients of variance

Re	$\overline{Nu}$	COV of $\overline{Nu}$ %
	$s/d = 2.83$ and $z/d = 2$	
12,000	80.8	29.8
15,000	101.3	31.2
18,000	108.0	30.1
	$s/d = 2.83$ and $z/d = 4$	
12,000	62.9	21.0
15,000	76.5	21.9
18,000	87.3	22.2
	$s/d = 2.83$ and $z/d = 6$	
12,000	50.3	31.9
15,000	58.4	32.9
18,000	65.1	33.4
	$s/d = 2.83$ and $z/d = 8$	
12,000	41.5	38.8
15,000	47.7	39.0
18,000	53.7	41.0
	$s/d = 4$ and $z/d = 2$	
12,000	72.2	27.7
15,000	84.3	28.5
18,000	97.1	29.2
	$s/d = 4$ and $z/d = 4$	
12,000	60.2	21.9
15,000	73.9	22.6
18,000	83.7	22.8
	$s/d = 4$ and $z/d = 6$	
12,000	52.2	24.8
15,000	59.4	24.7
18,000	72.0	26.1
	$s/d = 4$ and $z/d = 8$	
12,000	39.2	26.4
15,000	46.4	27.0
18,000	51.8	26.2
	$s/d = 6$ and $z/d = 2$	
12,000	50.4	27.8
15,000	57.7	29.8
18,000	64.0	30.7
	$s/d = 6$ and $z/d = 4$	
12,000	48.1	23.5
15,000	54.0	24.8
18,000	62.0	25.6
	$s/d = 6$ and $z/d = 6$	
12,000	42.9	24.4
15,000	50.7	24.6
18,000	57.9	25.2
	$s/d = 6$ and $z/d = 8$	
12,000	37.2	32.4
15,000	45.1	30.9
18,000	50.5	32.7

results of Chupp et al. compare well and the results agree within 10%. Figure 3b shows the comparison of average heat transfer coefficients estimated from the present data with the results reported by Chupp et al. for $D/d = 6$, $s/d = 4$, and $z/d = 1$. These results are seen to be higher than Chupp et al. by about 10–15%. This difference may be attributed to different thermal boundary conditions considered in the two investigations. Chupp et al. used constant temperature boundary condition, where as in present investigations it is constant heat flux. Chupp et al. have reported variation of about 15% in the Nusselt numbers when thermal boundary condition is changed from constant temperature to constant heat flux. These comparisons validate the apparatus and the technique of estimation of local heat transfer distribution.

Hence, the validated experimental setup was modified to accommodate two more rows of jet holes to carry out the heat transfer distribution on the curved surface.

V. Results and Discussions

An experimental investigation is carried out to study the local distribution of heat transfer coefficients due to the impingement of three rows of jets: one centrally and the other two at a 40° angle on either side of the centrally impinging row of jets on the cylindrical concave surface. The three rows of jets on the jet tube can be arranged either in staggered or inline fashion, as shown in Fig. 4. There is no significant change in the local heat transfer distribution between inline and staggered configurations as observed for $D/d = 10$, $s/d = 2.83$, and $z/d = 4$. Hence, influence of jet-to-plate distance z/d, jet-to-jet distance s/d, and Reynolds number is studied only for inline configuration for a curvature ratio D/d of 10. The spent fluid flow is constrained to exhaust in the streamwise directions along the passage on either side of the central line of jets of the concave surface.

A. Average Nusselt Number Distribution

The average Nusselt number for the entire cylindrical concave surface is estimated by averaging all the local Nusselt numbers arithmetically. It is a pixel-weighted average. The corresponding COV for each of the configurations is estimated to quantify the variation of the local Nusselt numbers about the average value. Figure 5 shows the influence of the Reynolds number on the average Nusselt numbers at different pitches. For all the jet tubes, the average Nusselt numbers increase with the increase in Reynolds number for a given jet-to-plate z/d distance. This is due to the fact that increase in Reynolds number increases the mass flow rate and hence the cooling capacity. Average Nusselt numbers decrease with the increase in jet-to-plate distance z/d for a given pitch s/d. This decrease in cooling with increase in z/d is because of the increase in flow interaction at larger jet-to-plate spacings. The average Nusselt numbers increases with the decrease in pitch s/d for a given jet-to-plate distance, due to the fact that the influence of jet increases per unit area and so does the

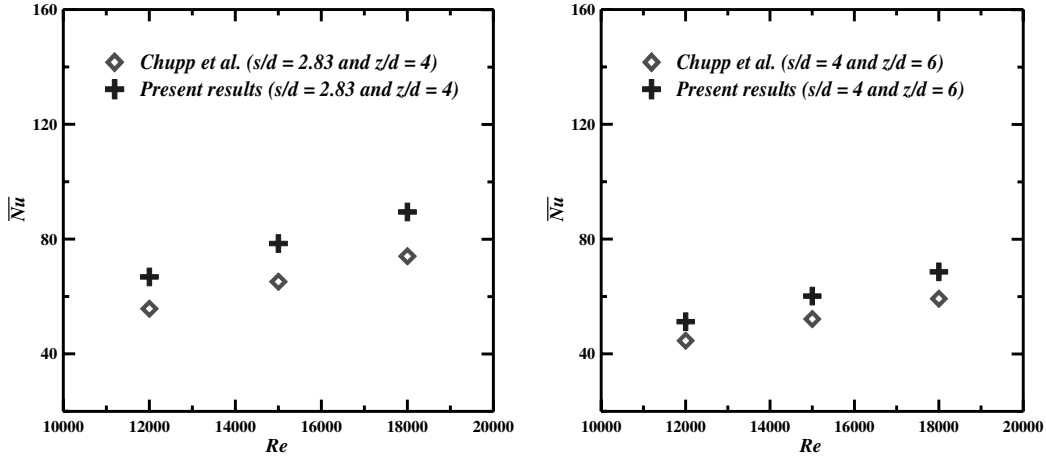

Fig. 6 Comparison of average Nusselt number correlations for the present case with Chupp et al. [1].

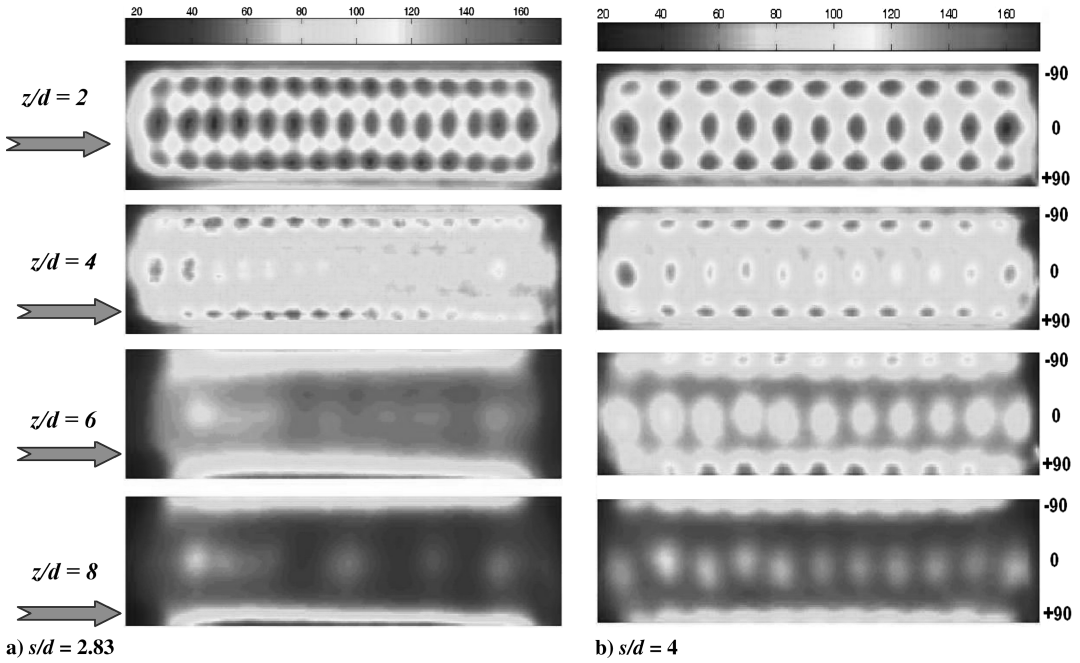

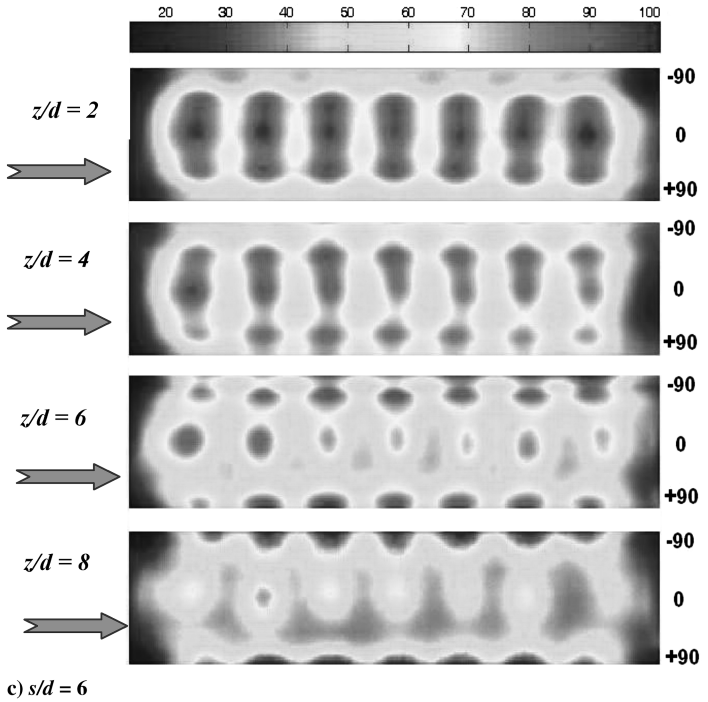

Fig. 7 Contour maps showing the distribution of local Nusselt number for the entire semicylindrical concave surface for $D/d = 10$ at a Reynolds number of 18,000.

average Nusselt number. Average Nusselt numbers can be correlated with the governing dimensionless parameters. The empirical correlation obtained using least-squares fit is given by Eq. (5). Since a boundary layer of constant thickness is formed at the stagnation region that extends along the chordwise region, the average Nusselt number is chosen in the following form, and the Prandtl number exponent is taken as 0.33:

$$\overline{Nu} = 0.2Re^{0.72}Pr^{0.33}\left(\frac{s}{d}\right)^{-0.44}\left(\frac{z}{d}\right)^{-0.28} \tag{5}$$

Equation (5) fits the experimental data within ±10% for 80% of the data points with a standard deviation of about 4%. Table 2 gives the average Nusselt number and the coefficient of variance of Nusselt numbers estimated for all configurations and Reynolds numbers studied. It is observed that COV of Nusselt numbers remains fairly constant for a given configuration at different Reynolds numbers. For a given pitch, COV of Nusselt numbers are maximum at $z/d = 2.0$ and with increase in z/d the COV of Nusselt numbers decreases. At a given jet-to-plate distance, the influence of pitch is seen to be marginal on COV of Nusselt numbers. The estimated values of COV can also be correlated with the governing dimensionless parameters. The empirical correlation obtained using least-squares fit is given by Eq. (6):

$$\text{COV} = 9.44Re^{0.13}\left(\frac{s}{d}\right)^{-0.08}\left(\frac{z}{d}\right)^{-0.1} \tag{6}$$

Equation (5) fits the experimental data within ±15% for 80% of the data points with a standard deviation of about 7.5%. The

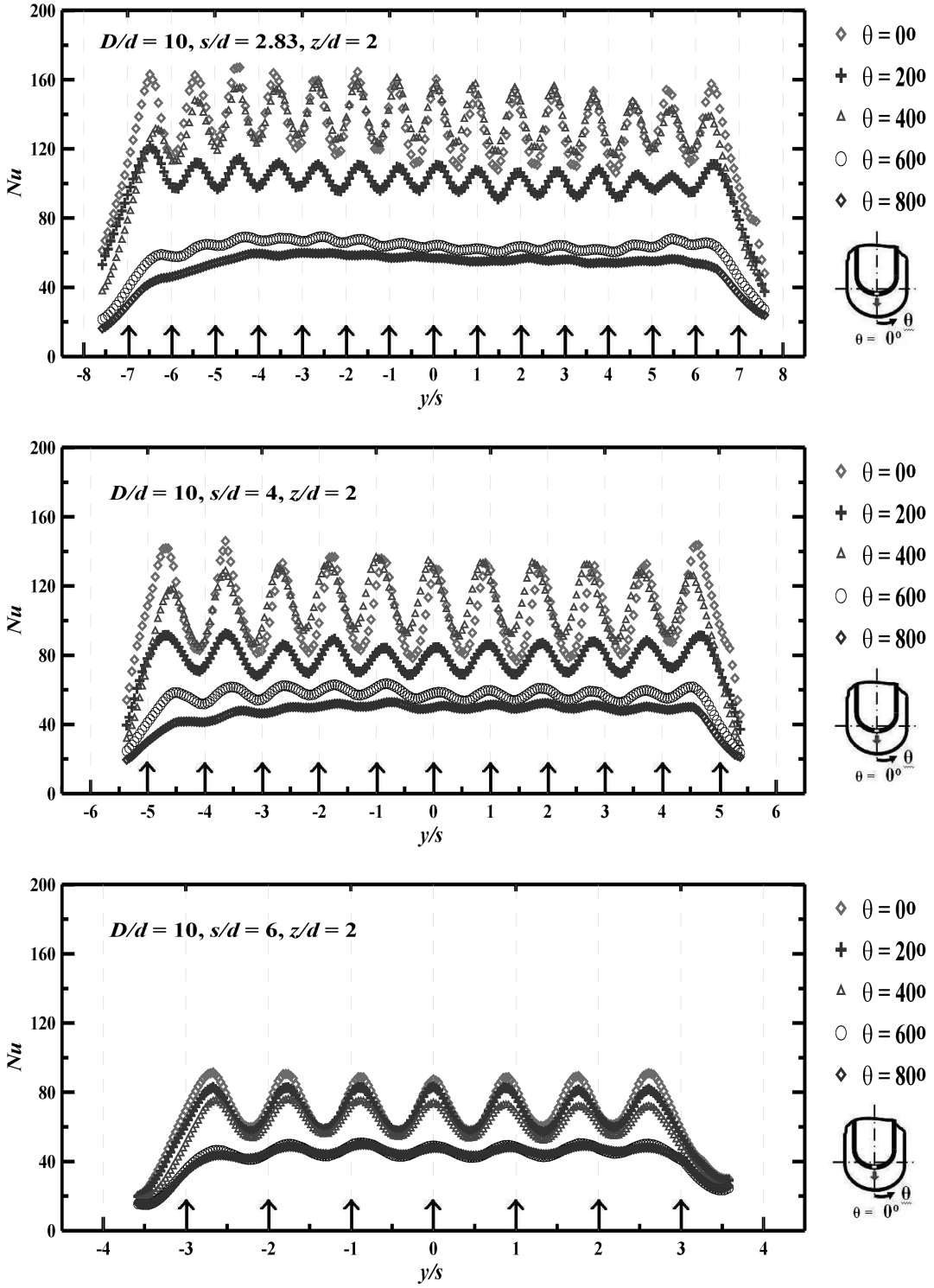

Fig. 8 Spanwise distribution of local Nusselt numbers at different circumferential locations for $D/d = 10$ and $z/d = 2$ for s/d of 2.83, 4, and 6 at $Re = 15,000$ for inline configuration.

correlation for the average Nusselt number for the present study was compared with that of Chupp et al. [1] for $2.83 \leq s/d \leq 6$, $2 \leq z/d \leq 6$, $12,000 \leq Re \leq 18,000$ and $D/d = 10$. These correlations were plotted against the Reynolds number and the plots for two such configurations are shown in Fig. 6. It was observed that the percentage deviation of the present results with that of Chupp et al. was within 20% for z/d greater than 2 and it was within 35% for z/d of 2 with the values for the present case being on the higher side. The high percentage deviation of the average Nusselt numbers could be due to the fact that there are two extra rows of jets on either side of the centrally machined row of jets.

B. Local Heat Transfer Distribution

Figure 7 shows the contour maps of the distribution of local Nusselt numbers for a Reynolds number of 18,000 for a $D/d = 10$ and for all s/d and z/d investigated. The air flow direction is from left to right and is indicated by the arrows in each of the contour maps. The stagnation points for each of the jet impingement can be identified as a region of peak Nusselt numbers along the spanwise central line ($\theta = 0°$) and two more on either side of the spanwise central line along the curvature ($\theta = 40$ and $-40°$). The exiting air for the jets along the central line gets opposed by the air exiting through the jets present in their adjacent row, and hence the curves are not

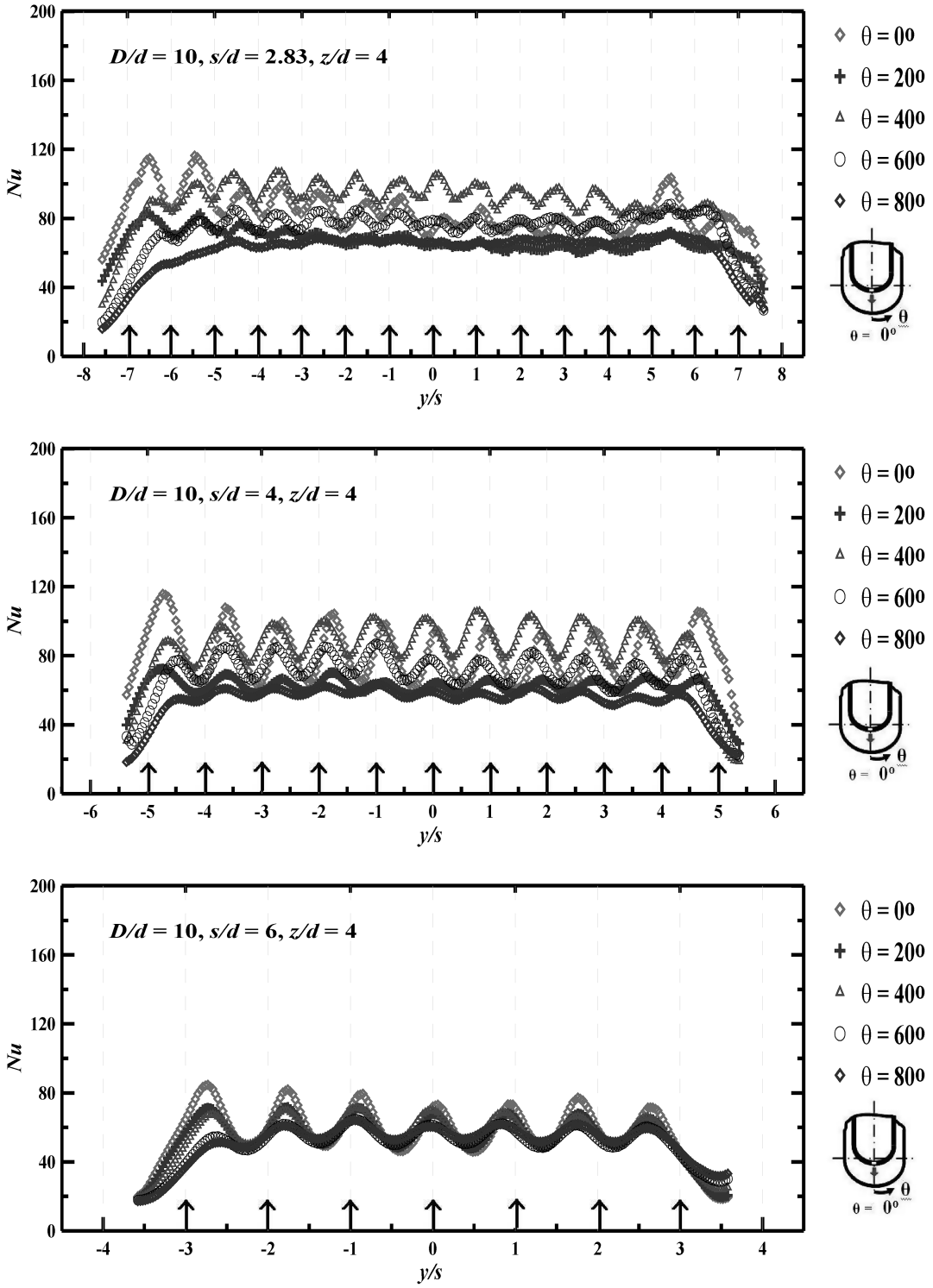

Fig. 9 Spanwise distribution of local Nusselt numbers at different circumferential locations for $D/d = 10$ and $z/d = 4$ for s/d of 2.83, 4, and 6 at $Re = 15,000$ for inline configuration.

stretched along the curvature. The contour maps show that the heat transfer coefficients decrease significantly with higher jet-to-plate distances along the spanwise rows of $\theta = -40$, 0, and 40°.

It should be noted that the target plate of diameter 30 mm and the jet tube of diameter 20 mm are not concentric at any of the jet-to-plate distances that were studied. Hence, the rows of jets at $\theta = -40$ and 40° on the jet tube do not impinge on the target plate at those angles.

Since the jet tube diameter is lower than the target plate diameter, the row of jets at $\theta = -40$ and 40° impinge away from the central line with a shift in the impingement varying with the jet-to-plate distances. The jet-to-plate distances of 2, 4, 6, and 8 that were considered were with respect to the central row of jets. The z/d for the rows of jets on either side of the central row of jets is lower than the z/d of the central jet.

It can be noted from Eq. (6) that the variation of COV with Reynolds number is less compared to average Nusselt number and the variation of COV with s/d and z/d is almost the same. The spanwise distribution of the local Nusselt numbers for Reynolds of 12,000, 15,000, and 18,000 and z/d of 2, 4, 6, and 8 on the semicircular concave surface at different circumferential positions along the curvature for the configurations from three jet tubes were studied and the results for $Re = 15,000$ are shown in Fig. 8–11. Each configuration is denoted by its curvature ratio, pitch and jet-to-plate ratio as (D/d, s/d, and z/d). The spanwise distances y are measured

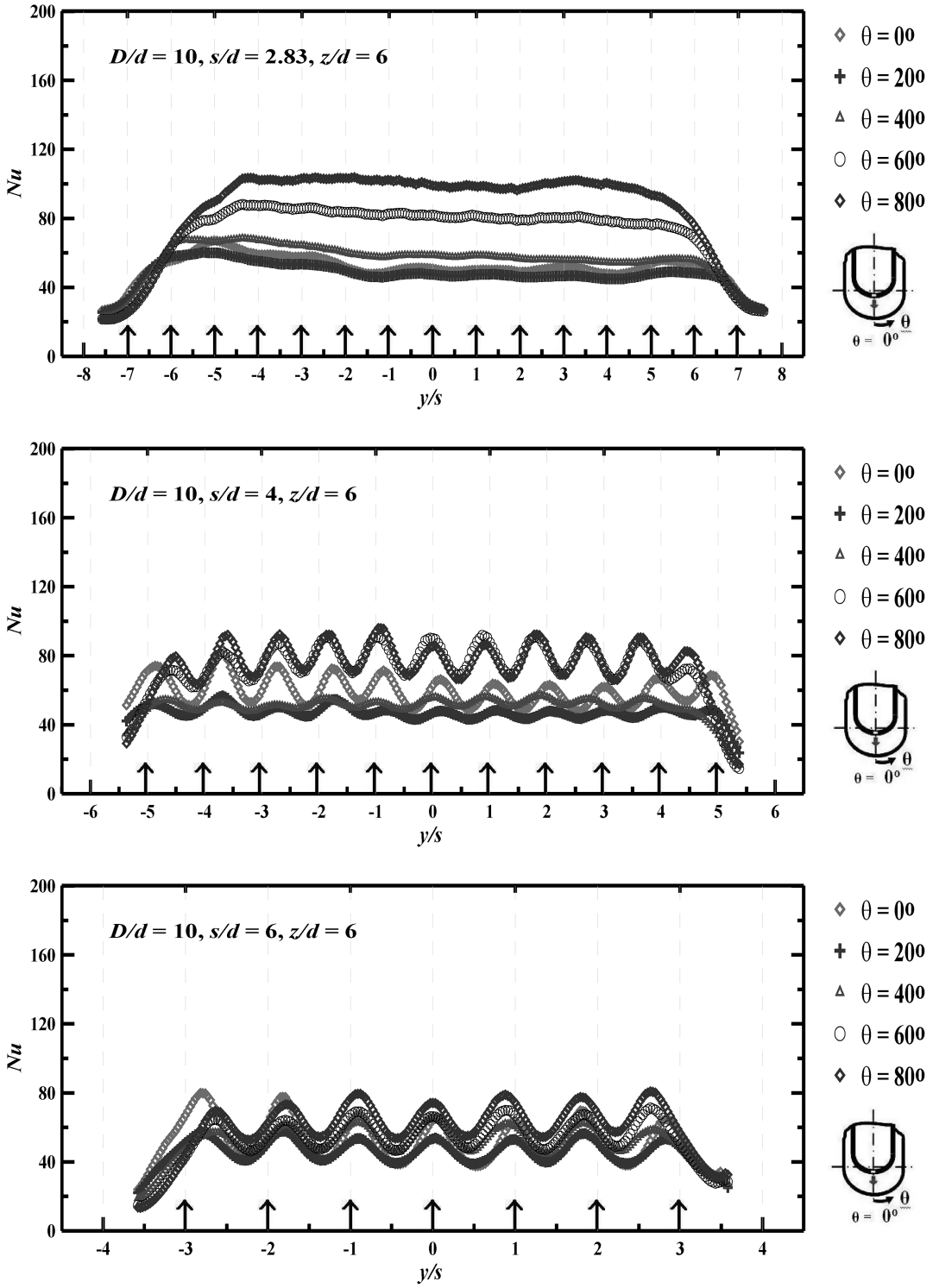

Fig. 10 Spanwise distribution of local Nusselt numbers at different circumferential locations for $D/d = 10$ and $z/d = 6$ for s/d of 2.83, 4, and 6 at $Re = 15,000$ for inline configuration.

from the midpoint of the spanwise central line. This point coincides with the axis of the central jet hole of the jet tube. The spanwise distances are normalized with the respective jet-to-jet distances s of the corresponding configuration. Hence, the reference coordinate at the midpoint of the spanwise central line is specified as $y/s = 0.0$. The locations of jets are shown in all the figures by the vertical arrows along the abscissa. The circumferential locations are identified as the angular positions on the curvature measured from the center of curvature of the target surface. That is, 0° corresponds to a circumferential position along the central spanwise line and ±90° correspond to a line along the end generators of the semicircular concave surface.

The distribution of heat transfer coefficients are seen to be symmetric about the central spanwise line. Hence, the local distribution of Nusselt numbers is shown along circumferential spanwise lines at 0, 20, 40, 60, and 80° on one half of the curved surface. In general, it is seen that for any configuration the heat transfer distribution shows a pattern of peaks and valleys along each of the spanwise lines from $\theta = 0$ to 80°. The peaks along the circumference, which correspond to a maximum Nusselt number, indicate the stagnation point due to the respective jet impingement from the row of jets adjacent to the spanwise central row of jets (the row of jets that are at $\theta = -40$ and 40° on the jet tube).

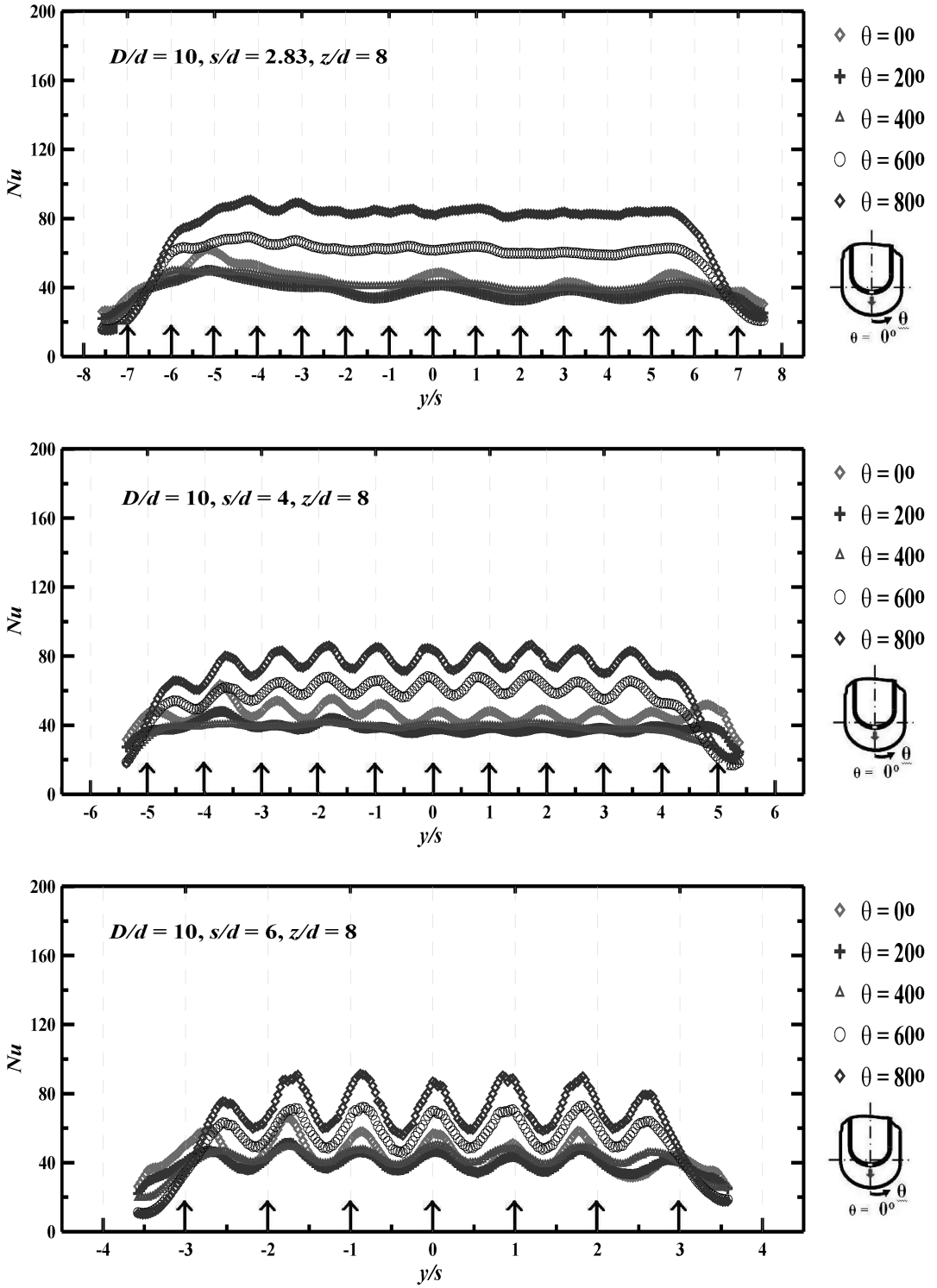

Fig. 11 Spanwise distribution of local Nusselt numbers at different circumferential locations for $D/d = 10$ and $z/d = 8$ for s/d of 2.83, 4, and 6 at $Re = 15,000$ for inline configuration.

The peaks along the 0° line indicate the stagnation point due to the respective jet impingement from the central row of jets (the row of jets that are at $\theta = 0°$ on the jet tube). The peaks along the other spanwise lines represent the Nusselt numbers along the circumferential line through the respective stagnation points. Valleys in the Nusselt number distribution along the spanwise lines indicate the location of minimum influence due to impinging jets and hence have minimum Nusselt number. These are normally seen midway between the circumferential lines through the successive peaks. It is observed for a given configuration of (D/d and z/d), the heat transfer coefficients all over the curved surface decrease with the increase in jet-to-jet distance. The decrease is more significant in the impingement region and not so much at other circumferential locations. This is also observed in contour maps.

C. Influence of Jet-to-Jet Distance on the Local Distribution of Heat Transfer Coefficients

The influence of s/d on the local distribution of heat transfer coefficient can be studied from Figs. 8–11. It is seen that, at $z/d = 2$ (Fig. 8), the peak values of Nusselt numbers are higher for lower pitches. For $s/d = 2.83$, 4, and 6, the difference in the peak Nusselt numbers along the circumferential locations $\theta = 0$, 20, and 40° is significant, but not those at $\theta = 60°$ and 80° where the influence of

pitch is almost negligible. The same phenomenon is observed for the minima values of Nusselt numbers (the valleys). This trend continues along the curvature till the edges. However, the Nusselt numbers all along the spanwise line near the edges remain almost same. Higher heat transfer coefficients observed midway between the circumferential lines through the stagnation points for lower s/d may be attributed to higher jet-to-jet interaction on the curved surface along the spanwise lines. For $z/d = 4$, 6, and 8, the influence of s/d is seen to be marginal on peak Nusselt numbers at all circumferential locations.

D. Influence of Jet-to-Plate Distance on the Local Distribution of Heat Transfer Coefficients

Local Nusselt numbers are discussed along circumferential spanwise lines at $\theta = 0$, 20, 40, 60, and 80°. For all the Reynolds numbers and s/d investigated, there seems to be a common trend observed for a particular z/d. For $z/d = 2$ (Fig. 8) the row of jets that are present at $\theta = -40$ and 40° locations on the jet tube now impinge on the target plate at an angle of $\theta = -42.5$ and 42.5°, respectively (since the jet tube and the target plate are not concentric). The maximum Nusselt numbers are seen at $\theta = 0$ and 40°. This is expected as the jet tube is nearest to the curved plate and the jet-to-plate distances for the row of jets at $\theta = 0$ and 40° are almost same (2 and 1.92). The next maximum is observed at an angle of $\theta = 20°$. This trend can be attributed to the streamwise flow of the fluid after impingement from the rows of jets present at $\theta = 0$ and 40°. The next maximum Nusselt number is at an angle of $\theta = 60°$ and the least Nusselt number is observed at an angle of at $\theta = 80°$. The influence of the row of jets present at $\theta = 40°$ are felt more at $\theta = 60°$ and hence has a higher Nusselt number compared to that at $\theta = 80°$. This trend should be expected as the mixing of fluid coming out from $\theta = 0$ and 40° does not take place much before impinging the plate.

For z/d of 4 (Fig. 9), the row of jets present at $\theta = -40$ and 40° locations on the jet tube now impinge on the target plate at angle of $\theta = -57.5$ and 57.5°, respectively. The jet-to-plate distances for the row of jets present at $\theta = 0$ and 40° on the jet tube are now 4 and 3.22, respectively. Hence, the maximum Nusselt numbers are seen at $\theta = 0$ and 40° same as that observed for z/d of 2. Again, much flow interaction is not seen and hence the air directly impinges onto the plate. The next maximum is seen to be at an angle of $\theta = 60°$ and this should be expected as the impingement shift due to nonconcentricity of the jet tube and target plate is evident and hence the heat transfer pattern at $\theta = 60°$. The next maximum Nusselt number comes at an angle of $\theta = 20°$. This is due to the fact that the circumferential distance on the impingement surface due to the jets at $\theta = 0$ and 40° is now increased and hence decrease of heat transfer coefficient at $\theta = 20°$ compared to that at $\theta = 60°$. The Nusselt numbers at $\theta = 80°$ is more or less equal to that at $\theta = 20°$ as influence of jet is not much felt at that location.

For z/d of 6 (Fig. 10), the row of jets present at $\theta = -40$ and 40° locations now impinge on the target plate at angle of $\theta = -73.85$ and 73.85°, respectively. Hence, the maximum Nusselt numbers are seen at $\theta = 60°$ and 80°. The jet-to-plate distance for the row of jet at $\theta = 40°$ is 4.14, but not 6, and hence the enhancement of heat transfer at $\theta = 60$ and 80°. It should be obvious that the next maximum Nusselt number occurs at $\theta = 0°$ as the row of jets on the central line are at a z/d of 6, which is at a larger distance compared to those on either side of the central line. The jets impinging at $\theta = 0$ and 73.85° undergo mixing before impinging the plate, and hence the Nusselt numbers at locations of $\theta = 20$ and 40° are almost equal.

For z/d of 8 (Fig. 11), the row of jets present at $\theta = -40$ and 40° locations now impinge on the target plate at angle of $\theta = -94.5$ and 94.5°, respectively. Hence, the maximum Nusselt numbers are seen at $\theta = 80°$. The jet-to-plate distances for the row of jets on either side of the central row of jets are 4.42, but not 8, and hence the enhancement of heat transfer at $\theta = 80°$. Similar argument is used to say that the next maximum Nusselt number occurs at an angle of $\theta = 60°$, due to the lowered jet-to-plate distances for the row of jets present at an angle of $\theta = 40°$ on the jet tube. Similar as in the case for z/d of 6 the next maximum is seen at $\theta = 0°$, due to the presence of the central row of jets. The magnitude is lesser than compared to that at $\theta = 60$ and 80° and is due to the reduced jet-to-plate distance for the row of jets on either side of the central line. Again, due to the flow mixing between the two rows of jets the Nusselt numbers at $\theta = 20$ and 40° are almost equal.

The successive maxima and minima at each of the spanwise location are not consistent. For $s/d = 2.83$, the difference in their respective maxima and minima at $\theta = 0$ and 40° are very high compared to that at $\theta = 20$, 60, and 80° for z/d of 2 and 4. At $\theta = 20°$ the difference is lower but significant. At 60° the difference between maxima and minima is diminished but still perceivable. At $\theta = 80°$ the difference between the maxima and minima is almost negligible for $z/d = 2$ but significant enough for $z/d = 4$. At $z/d = 6$ and 8 there is a very high jet-to-jet interaction, and hence the difference between the successive maxima and minima at each of the spanwise lines is almost negligible, and hence the Nusselt number is constant throughout the spanwise line at each of the circumferential location.

For $s/d = 4$, a similar pattern as seen at $s/d = 2.83$ is observed for the difference between the successive maxima and minima for z/d of 2 and 4. For z/d of 6 and 8 the difference between the successive maxima and minima is significant with the maximum difference occurring at $\theta = 60$ and 80°. The difference at $\theta = 0°$ is a little lower, and for the locations of $\theta = 20$ and 40°, it is almost negligible. This effect is more pronounced for $z/d = 8$ than at 6. For $s/d = 6$, the jet-to-jet distance is large, and hence the jet-to-jet interaction is minimum and there is a considerable difference in successive maxima and minima at the spanwise lines. This is observed at all z/d and at all circumferential positions investigated. For z/d of 6 and 8 the trend is similar to that observed at $s/d = 4$, but the difference

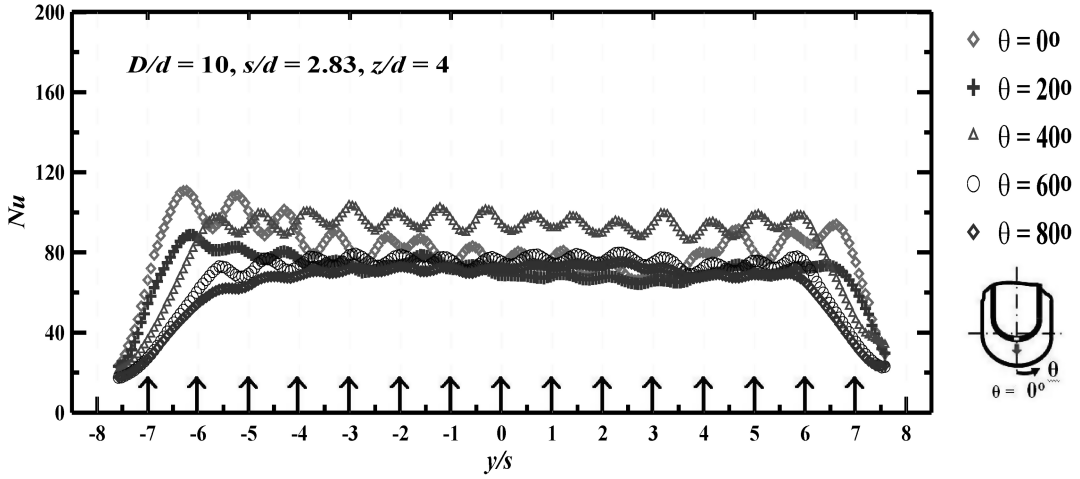

Fig. 12 Spanwise distribution of local Nusselt numbers at different circumferential locations for $D/d = 10$ $s/d = 2.83$ and $z/d = 4$ at a Reynolds number of 15,000 for staggered configuration.

Table 3 Comparison of average Nusselt numbers and their coefficient of variance for inline and staggered configurations at $s/d = 2.83$

Configuration		$\overline{Nu}$		COV of $\overline{Nu}$ %	
z/d	Re	Inline	Staggered	Inline	Staggered
4	12,000	62.9	63.1	21.0	22.4
4	15,000	76.5	75.1	21.9	24.5
4	18,000	87.3	86.4	22.2	25.6

between successive maxima and minima are more pronounced, due to the decreased jet-to-jet interactions.

E. Influence of Arrangement of Jets (Staggered and Inline)

Figure 12 shows the local heat transfer distribution for $D/d = 10$, $s/d = 2.83$, and $z/d = 4$ with jets arranged in staggered configuration at a Reynolds number of 15,000. These results may be compared with the corresponding inline configuration shown in Fig. 8.

It can be observed that the Nusselt number distribution is almost similar to that of the inline jet configuration. Table 3 gives a comparison between the average Nusselt number and COV for the inline and staggered configuration. It can be observed that there is no significant change in the staggered and the inline values, and hence the investigations were limited to the inline configurations.

VI. Conclusions

An experimental investigation is carried out to study the local distribution of heat transfer coefficients, due to the impingement of three rows of jets on a semicylindrical concave surface. Three jet-to-jet distances of $2.83d$, $4d$, and $6d$ were considered for the present study. Four different jet-to-plate distances of $2d$, $4d$, $6d$, and $8d$ were considered for the configuration of each of these three jet tubes. The curvature ratio D/d is kept constant as 10. The jet Reynolds number is varied from 12,000 to 18,000 for all the configurations studied. The following conclusions are inferred from the present study.

1) The Nusselt number contours due to each jet are distributed symmetrically on either side of the spanwise central line. However, the spread of the heat transfer coefficients along the curvature and the longitudinal direction are not similar.

2) The overall average Nusselt numbers increase with the increase in Reynolds number. And they decrease with increase in jet-to-plate distances for a given jet tube at a given Reynolds number. But the influence of s/d on the overall average Nusselt number is marginal for a $z/d = 8$ at all Reynolds numbers.

3) Lower jet-to-plate distances and smaller jet-to-jet spacing generate higher values of average heat transfer coefficients. Lower jet-to-plate distance and higher jet-to-jet spacing leads to higher values of COV indicating a larger degree of nonuniformity of Nusselt number distribution. The configuration (10, 2.83, and 4) has a higher average Nusselt number with a lower COV compared to the rest of the values. The empirical correlation obtained using least-squares fit for average Nusselt number and COV is given by

$$\overline{Nu} = 0.2Re^{0.72}Pr^{0.33}\left(\frac{s}{d}\right)^{-0.44}\left(\frac{z}{d}\right)^{-0.28} \tag{5}$$

$$\text{COV} = 9.44Re^{0.13}\left(\frac{s}{d}\right)^{-0.08}\left(\frac{z}{d}\right)^{-0.1} \tag{6}$$

4) The local heat transfer coefficients at $\theta = 0^\circ$ decrease with increase in z/d at all Reynolds numbers, whereas the heat transfer coefficients at $\theta = 60$ and 80° increase with increase in z/d at all Reynolds numbers. This is due to the fact that the jet tube and the target plate surface are not concentric and the row of jets on either side of central row of jets impinge toward $\theta = 60$ to 80° with the increase in z/d.

5) Local heat transfer coefficients decrease with the increase in jet-to-jet distances for a given jet-to-plate distance and Reynolds number. The difference in the Nusselt number peaks with the increase in pitch is significant for $\theta = 0$, 20, and 40°, but not at $\theta = 60$ and 80°, where the influence of pitch is almost negligible. The same phenomenon is observed for the minima values of Nusselt numbers.

6) The Nusselt numbers all along the spanwise line near the edges remain almost same. Higher heat transfer coefficients observed midway between the stagnation points for lower s/d may be attributed to higher jet-to-jet interaction on the curved surface along the spanwise lines.

References

[1] Chupp, R. E., Helms, H. E., McFadden, P. W., and Brown, T. R., "Evaluation of Internal Heat-Transfer Coefficients for Impingement-Cooled Turbine Airfoils," *Journal of Aircraft*, Vol. 6, No. 3, May–June 1969, pp. 203–208. doi:10.2514/3.44036

[2] Metzger, D. E., Yamashita, T., and Jenkins, C. W., "Impingement Cooling of Concave Surfaces with Lines of Circular Air Jets," *Journal of Engineering for Power*, Vol. 81, July 1969, pp. 149–158.

[3] Metzger, D. E., Baltzer, R. T., and Jenkins, C. W., "Impinging Cooling Performance in Gas Turbine Airfoils Including Effects of Leading Edge Sharpness," *Journal of Engineering for Power*, Vol. 94, No. 3, July 1972, pp. 219–225.

[4] Jusionis, V. J., "Heat Transfer from Impinging Gas Jets on an Enclosed Concave Surface," *Journal of Aircraft*, Vol. 7, Jan.–Feb. 1970, pp. 87–88. doi:10.2514/3.44127

[5] Tabakoff, W., and Clevenger, W., "Gas Turbine Blade Heat Transfer Augmentation by Impingement of Air Jets Having Various Configurations," *Journal of Engineering for Power*, Vol. 94, Jan. 1972, pp. 51–60.

[6] Bunker, R. S., and Metzger, D. E., "Local Heat Transfer in Internally Cooled Turbine Airfoil Leading Edge Regions: Part I, Impingement Cooling Without Film Cooling Extraction," *Journal of Turbomachinery*, Vol. 112, 1990, pp. 451–458. doi:10.1115/1.2927680

[7] Iacovides, H., Kounadis, D., Launder, B. E., Li, J., and Xu, Z., "Experimental Study of Flow and Thermal Development of a Row of Cooling Jets Impinging on a Rotating Concave Surface," *Journal of Turbomachinery*, Vol. 127, Jan. 2005, pp. 222–229. doi:10.1115/1.1812778

[8] Fenot, M., Vullierme, J. J., and Dorignac, E., "Local Heat Transfer Due to Several Configurations of Circular Air Jets Impinging on a Flat Plate with and Without Semi Confinement," *International Journal of Thermal Sciences*, Vol. 44, 2005, pp. 665–675. doi:10.1016/j.ijthermalsci.2004.12.002

[9] Hrycak, P., "Heat Transfer from a Row of Impinging Jets to Concave Cylindrical Surface," *International Journal of Heat and Mass Transfer*, Vol. 24, 1981, pp. 407–419. doi:10.1016/0017-9310(81)90048-X

[10] Taslim, M. E., Setayeshgar, L., and Spring, S. D., "An Experimental Investigation of Advanced Leading Edge Impingement Cooling Concepts," *Journal of Turbomachinery*, Vol. 123, 2001, pp. 147–153. doi:10.1115/1.1331537

[11] Taslim, M. E., and Khanicheh, A., "Experimental and Numerical Study of Impingement on an Airfoil Leading Edge with and Without Showerhead and Gill Film Holes," *Transactions of the ASME*, Vol. 128, 2006, pp. 310–320. doi:10.1115/1.2137742

[12] Rama Kumar, B. V. N., and Prasad, B. V. S. S. S., "Experimental and Computational Study of Multiple Circular Jets Impinging on a Concave Surface," *Proceedings of the 33rd National and 3rd International Conference on Fluid Mechanics and Fluid Power*, Indian Institute of Technology, Bombay, India, Dec. 2006.

[13] Moffat, R. J., "Describing the Uncertainties in Experimental Results," *Experimental Thermal and Fluid Science*, Vol. 1, 1988, pp. 3–17. doi:10.1016/0894-1777(88)90043-X